Journal of Materials Chemistry A

Accepted Manuscript

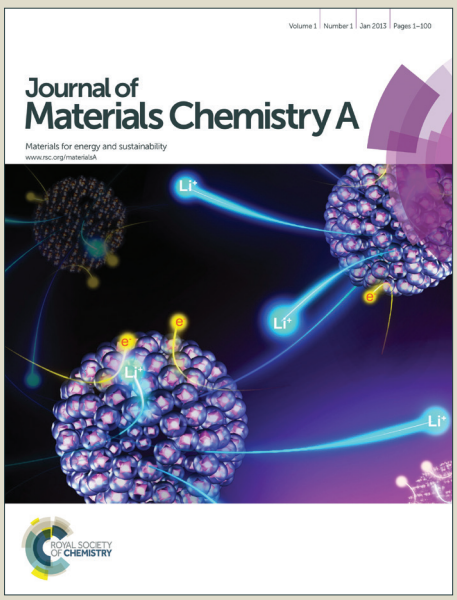

ROYAL SOCIETY OF CHEMISTRY

www.rsc.org/materialsA

Article Manuscript for ***Journal of Materials Chemistry A***

$Na_{2.44}Mn_{1.79}(SO_4)_3$: A new member of *alluaudite* family of insertion compounds for sodium ion batteries

Debasmita Dwibedi,[‡] Rafael B. Araujo,[Ø] Sudip Chakraborty,[Ø]
Pradeep P. Shanbogh,[+] Nalini G. Sundaram,[+]
Rajeev Ahuja,[Ø] and Prabeer Barpanda[‡]*

[‡] Faraday Materials Laboratory, Materials Research Centre,
Indian Institute of Science, C.V. Raman Avenue, Bangalore, 560012, India.

[Ø] Condensed Matter Theory Group, Department of Physics and Materials Science,
Uppsala University, P.O. Box 530, SE-751 21 Uppsala, Sweden.

[+] Materials Science Division, Poornaprajna Institute of Scientific Research,
Bidalur post, Devanahalli, Bangalore, 562164, India.

* prabeer@mrc.iisc.ernet.in
Phone: +91-80-2293-2873; Fax: +91-80-2360-7316

Abstract

Sodium-ion batteries have been extensively pursued as economic alternatives to Lithium-ion batteries. Investigating the polyanion chemistry, *alluaudite* structured $Na_2Fe^{II}_2(SO_4)_3$ has been recently discovered as a 3.8 V positive electrode material (Barpanda *et al*, *Nature Commun*., 5:4358, 2014). Registering the highest ever Fe^{III}/Fe^{II} redox potential (vs. Na/Na^+) and formidable energy density, it has opened up a new polyanion family for sodium batteries. Exploring the *alluaudite* family, here we report isotypical $Na_{2+2x}Mn^{II}_{2-x}(SO_4)_3$ (x = 0.22) as a novel high-voltage cathode material for the first time. Following low-temperature (ca. 350°C) solid-state synthesis, the structure of this new *alluaudite* compound has been solved adopting a monoclinic framework (s.g. *C*2/*c*) showing antiferromagnetic ordering at 3.4 K. Synergising experimental and *ab-initio* DFT investigation, $Na_{2+2x}Mn^{II}_{2-x}(SO_4)_3$ has been found to be a potential high-voltage (ca. 4.4 V) cathode material for sodium batteries.

Keywords: sodium-ion battery, *alluaudite*, $Na_2Mn_2(SO_4)_3$, susceptibility, DFT study.

1. Introduction

Rechargeable batteries have become ubiquitous in modern life empowering suites of consumer electronics, plug-in (hybrid) electric automobiles and grid power storage. Taking advantage of their lightweight induced high gravimetric/ volumetric energy density, Li-ion batteries have conquered mobile energy devices constrained by size/ weight restriction. However, the growing concern over cost and availability of lithium resources has encouraged the usage of batteries based on alternate carrier ions (e.g. Na).[1] Specially the economy, abundance and uniform geographic distribution of sodium resources have paved way for large-scale implementation of sodium-ion batteries such as grid power storage. Thus, following a two-decade long hibernation of research on sodium containing oxides (e.g. Na_xCoO_2)[2], there has been renewed interest in oxides (e.g. Na_xVO_2, Na_xCrO_2, $Na_x[Fe_{1/2}Mn_{1/2}]O_2$, $Na[Ni_{1/3}Mn_{1/3}Co_{1/3}]O_2$) and polyanionic (e.g. $Na_3V_2(PO_4)_3$, $NaFeSO_4F$, $Na_2FeP_2O_7$, Na_2FePO_4F) insertion materials for Na-ion batteries (Ref.1 and references therein).

One major concern with sodium batteries is the general observations of low redox potential owing to the difference between Li/Li^+ (- 3.04 V vs. SHE) vis-à-vis Na/Na^+ (- 2.71 V vs. SHE). This is even more serious in case of polyanionic system having inherently lower theoretical capacity (Q_{Th}) owing to the weight penalty stemming from spectator ions. It can be compensated by new polyanionic chemistries with highly electronegative SO_4-based units. Based on inductive effect[3], sulfate-based cathode systems have been shown to deliver the highest redox potential (e.g. Fe^{3+}/Fe^{2+} redox potential of 3.9 V vs Li/Li^+).[4-6] Using the sulphate-chemistry for Na-based systems, recently Yamada group has reported an *alluaudite* structured $Na_2Fe_2(SO_4)_3$ as a 3.8 V cathode material offering excellent rate kinetics and energy density.[7,8] This new compound has opened up a completely new class of insertion materials to design novel cathode materials. At this stage, in an effort to enlarge the *alluaudite* family, we have unveiled $Na_{2+2x}Mn_{2-x}(SO_4)_3$ (x = 0.22) as a novel potential high-voltage cathode for sodium-ion batteries. Here, we describe the low-temperature synthesis, crystal structure, magnetic transition and electronic/ electrochemical properties of this new material offering promise as a high-voltage sustainable sodium insertion system.

2. Experimental Section

2.1 ***Material Synthesis:*** The target product, $Na_{2+2x}Mn_{2-x}(SO_4)_3$, was synthesized by taking an off-stoichiometric 3:4 molar mixture of Na_2SO_4 (Merck, 99.5%) and in-house prepared $MnSO_4$ precursors. The anhydrous $MnSO_4$ was prepared by

calcination of commercially procured hydrated $MnSO_4.5H_2O$/ $MnSO_4.H_2O$ (Sigma-Aldrich, 99%) precursors either at 200 °C for 6 h under primary vacuum or at 250-300 °C for 2 h inside an Ar-filled tube furnace. Precalculated amount of Na_2SO_4 and anhydrous $MnSO_4$ were intimately mixed by (dry) planetary milling for 6 h (at 350 rpm) employing Cr-hardened stainless steel (Cr-SS) milling media and container. Following, this mixture was annealed at 350 °C for 6-12 h (under steady Ar flow) to obtain the final product.

***2.2 Structural and Physical Characterization*:** High-resolution powder XRD pattern was collected with a PANalytical X'Pert Pro diffractometer using a Cu-Kα source (λ_1 = 1.5405 Å, λ_2 = 1.5443 Å) operating at 40 kV/ 30 mA and a Lynx Eye positional detector. Typically, XRD patterns were collected in the 2θ range of 5~90° (step size of 0.45°.min^{-1}). Rietveld refinement[9] of the XRD pattern was conducted using the GSAS program using EXPGUI, a graphical interface of the program GSAS.[10-11] The background was refined using a shifted Chybeshev polynomial function and the diffraction profile was fitted by a pseudo-Voigt function. The elemental composition of target product was determined using inductively coupled plasma atomic emission spectroscopy (ICP) with a PerkinElmer Optima 8300 spectrometer. The morphology and elemental mapping of as-synthesized sample, sprinkled on carbon tape, was analyzed with an FEI Inspect F50 scanning electron microscope operating at 5-20 kV. Following, transmission electron microcopy was performed with an FEI Tecnai F30 S-Twin unit (operating at 200 kV) by adding few drops of powder sample soaked in acetone on a copper grid. FT-Infrared spectrum of powder sample (in KBr pellet) was acquired by an Agilent Cary 660-FTIR spectrometer in the wavenumber range of 400-4000 cm^{-1} (number of cycles = 4). The thermogravimetric (TGA) data were acquired with a TA Q-50 unit in the temperature range of 25-900 °C (under steady N_2 flow).

***2.3 Magnetic Susceptibility Analysis*:** The magnetic susceptibility measurements were conducted with a Quantum Design physical property measurement system (PPMS) equipped with a vibrating sample magnetometer (VSM) option. The magnetization was recorded in field cooled (FC) mode with varied applied external magnetic field (H) in the temperature range 2–300 K. Magnetization as a function of field was measured at 2 K over 6 segments to ±10 kOe.

***2.4 Computational Methodology*:** Density functional theory (DFT) based *ab-initio* calculations was carried out by employing the projector Augmented Wave method as implemented in the Vienna *ab-initio* Simulation Package (VASP).[12,13] The calculations have been undertaken by using the spin-polarized formalism in the Perdew, Burke, and Ernzerhof (PBE) parameterization for the exchange and correlation functional.[14] Heyd-Scuseria-Ernzerhof (HSE06)[17,18] that is a fractional mixture of an exact Hartree-Fock exchange is also employed to compensate the self-interaction error. An energy cut-off of 600 eV was employed together with a gamma-centered k-point of 4x4x6. The magnetic configuration of $Na_2Mn_2(SO_4)_3$ are also investigated and in most of the cases the antiferromagnetic state becomes the more stable configuration with a very small energetic difference with respect to the ferromagnetic magnetic configuration.

3. Results and Discussion

3.1 Crystal structure and material stability:

Unlike the PO_4-containing *alluaudite* materials [AMnFe$_2$(PO$_4$)$_3$; A = Li/ Na][19], the SO_4-based *alluaudite* materials tend to form off-stoichiometric phases such as $Na_{2+2x}Fe_{2-x}(SO_4)_3$.[7-8] In the Na_2SO_4-MSO_4 binary system, material synthesis leads to some unreacted MSO_4, which can be reduced by excess usage of Na_2SO_4 that invariably yields off-stoichiometric phases. Similar to the Fe-case, it was futile to conduct synthesis using stoichiometric amounts of precursors (i.e. 1:2 molar ratio of Na_2SO_4 and $MnSO_4$), invariably forming product rich with impurities (e.g. $MnSO_4$). So, we employed Na_2SO_4 excess precursor mixture (i.e. 3:4 molar ratio of Na_2SO_4 and $MnSO_4$) to obtain the desired *alluaudite* phase. As the SO_4-based compounds intrinsically suffer from rapid thermal decomposition above 400-450 °C releasing SO_x (x = 2, 3) gases, we restricted the final annealing temperature to 350 °C. It led to the formation of desired phase with a trace amount of Mn-S-O impurities (e.g. $MnSO_4$). The crystal structure of this *hitherto* unknown compound was refined via Rietveld method using high-resolution X-ray diffraction (HR-XRD) pattern. The observed, calculated and difference fit for the refinement are shown in **Figure 1**. It was found to be isostructural to the Fe-homologue assuming an *alluaudite* mineral structure having a monoclinic framework (s.g. $C2/c$, #15). Using isostructural $Na_{2.4}Fe_{1.8}(SO_4)_3$ as a model structure,[7-8] the atomic positions, occupancy and thermal parameters of Na, Mn and O atoms were refined. Overall, Rietveld refinement led to the off-stoichiometric composition of $Na_{2.44}Mn_{1.79}(SO_4)_3$. The off-stoichiometry between Na and Mn was

further confirmed by ICP analysis, which determined the Na/Mn elemental ratio to be 1.36 that is close to Rietveld derived value of 1.363. The final crystallographic data is summarised in **Table 1** (.cif file provided in the supporting information).

The $Na_{2.44}Mn_{1.79}(SO_4)_3$ forms a new member of SO_4-based *alluaudite* with general formula $AA'BM_2(SO_4)_3$, where *A* and *A'* are partially occupied Na (Na2 and Na3), B is fully occupied Na (Na1) and *M* is partially occupied Mn (Mn1). As shown in **Figure 2a**, the framework is built with distorted MnO_6 octahedral building blocks with all Mn occupying a crystallographically distinct site. The degree of distortion (Δ) in this alluaudite framework can be quantified as: $\Delta = 1/6 \sum_{n=1,6} \{(d_n - \langle d \rangle)/\langle d \rangle\}^2$, where d_n and d are individual Mn–O bond lengths and the average Mn–O bond length respectively. In case of $Na_{2.44}Mn_{1.79}(SO_4)_3$, the distortion value was found to be 5.66 ($\times 10^{-4}$), which is much higher than the distortion value of 3.46 ($\times 10^{-4}$) found in isostructural $Na_{2.2}Fe_{1.8}(SO_4)_3$. This enhanced distortion can be ascribed to the larger cationic size of Mn^{2+} (0.90 pm-MnO_6 high-spin) vis-à-vis Fe^{2+} (0.78 pm-FeO_6 high-spin).[20] These adjacent distorted MnO_6 octahedra share equatorial edge to form isolated Mn_2O_{10} dimers (Fig. 2b), which are in turn linked by isolated SO_4 tetrahedra strictly in corner-sharing fashion to form a three-dimensional structure delimiting large cavities along *c*-axis. The Na atoms are accommodated inside these cavities, coordinated with O atoms from surrounding SO_4 tetrahedral units (Fig. 2c). Two distinct kinds of large cavities are observed accommodating Na2 and Na3 sites. These tunnels can favour the swift (de)insertion of Na-cations. The crystal structure was further validated by calculating the bond-valence-sum (BVS) values using the Zachariasen formula $BVS = \sum \exp [(d_o - d_i)/ B]$, where d_i is the bond lengths between adjacent cation-anion pairs, B = 0.37 and d_o is an empirically determined parameter for specific cation-anion pairs.[21] We noticed good agreement between BVS values and valency state of individual elements proving the veracity of structure (Table 1). It is worth noting while the BVS values of Na1 (1.2190) and Na2 (0.988) are close to the expected value (i.e. 1), the BVS value of Na3 (i.e. 0.5832) is much lesser than its valency. It indicates shallow site potential for Na^+ occupation in Na3 sites (i.e. relatively unstable) that can favour fast Na^+ ion diffusion during cathode operation. These features are quite similar to isostructural Fe-homologue.

The morphology of the solid-state synthesized $Na_{2.44}Mn_{1.79}(SO_4)_3$ product was analysed by electron microscopy. As shown in **Figure 3**, large micrometric (1-5 μm) agglomerates are observed, which consist of near spherical nanometric (50~100 nm) particles. This nanoscale morphology can be rooted to the low-temperature annealing

(ca. 350 °C) involving less aggressive grain-growth and developing smaller particles. The elemental mapping captures all expected elements with uniform distribution (**Figure 4**). In sync with the structural analysis, the elemental mapping confirms the off-stoichiometry in alluaudite phase, which is Na-rich and Mn-deficient as evident from Fig. 4 c and d. The nanoscale morphology can facilitate electrochemical activity.

The structural features were also probed with infrared spectroscopy. As shown in **Figure 5**, despite the hygroscopic nature of SO_4-compounds, no signature of any surface adsorbed moisture was noticed as confirmed by the absence of any peak ~ 3500 cm^{-1} (stemming from symmetric/ asymmetric stretching of OH^- species). At low wavenumber region, fingerprint peaks related to SO_4^{2-} species were observed. Overall, three distinct kinds of infrared bands were observed: two from stretching vibration of SO_4 units [symmetric stretching ν_1 ~ 983 cm^{-1} and asymmetric stretching ν_3 ~ 1100 cm^{-1}] and one from bending vibration of SO_4 units [asymmetric bending ν_4 ~ 620 cm^{-1}]. This FTIR analysis confirms the formation of pristine SO_4-rich material, devoid of any surface-adsorbed moisture.

Following, the material stability was tested by thermogravimetric analysis. Although sulphate-containing compounds are prone to decomposition upon heating, the $Na_{2.44}Mn_{1.79}(SO_4)_3$ compound was found to be stable until 600 ºC, when it starts decomposing to release SO_x gases (**Figure 6**). However, the net weight loss is limited to only 10 wt% until 900 ºC. It offers excellent thermal stability when compared to isotypical $Na_{2+2x}Fe_{2-x}(SO_4)_3$, where the onset of decomposition starts ~ 450 ºC leading to significant weight loss over 30 wt%. Similar trend (Mn > Fe) in thermal stability is noticed in fluorosulphate (AMSO$_4$F; A = Li/ Na) family of SO_4-compounds.[22, 23] As expected for all SO_4-containing materials, the $Na_{2.44}Mn_{1.79}(SO_4)_3$ compound dissolves completely in water. Further, it is prone to ambient poisoning over a prolonged period. The material degradation was studied for one calendar year. Visible material degradation was noticed as evident from the appearance of new peaks in the XRD and FTIR analyses (Supporting information). Over a year, the material completely disintegrates to form a mixture of Na-Mn-S-O phases (such as $Na_6Mn(SO_4)_4$, $MnSO_4$, Na_2SO_4, $Na_2Mn(SO_4)_2.4H_2O$, $MnSO_4.xH_2O$ etc). This type of ambient poisoning is well known and is expected to be more severe in the isostructural Fe-alluaudite case. Thus, these alluaudite phases should be kept under inert atmosphere for safe handling.

3.2 Magnetic properties:

The presence of 3*d* transition metal (Mn) renders magnetic characteristics to *alluaudite* $Na_{2.44}Mn_{1.79}(SO_4)_3$. Its magnetic field dependence of magnetization (i.e. M-H curve) is shown in **Figure 7**. At room temperature (300 K), paramagnetic nature is observed (Fig. 5a), while an antiferromagnetic character is noticed at low temperature (2 K) as evident from S-curve (Fig. 5b). The absence of any hysteresis suggests the absence of any ferromagnetic component, but the occurrence of antiferromagnetic ordering. **Figure 8** shows the temperature dependence of the magnetic susceptibility (χ) of $Na_{2.44}Mn_{1.79}(SO_4)_3$ between 300 K and 2 K in a zero-field cooled (ZFC) mode using an applied field (H) of 1000 Oe. It depicts an antiferromagnetic transition (AFM) at very low temperature $T_N \sim 3.4$ K (Figure 6, inset).

A linear fit of the inverse molar magnetic susceptibility χ^{-1} to the paramagnetic region ($50 \leq T \leq 250$ K) shows a Curie-Weiss behaviour with a Curie constant C = 0.0216 emu K/g. It corresponds to an effective moment $\mu_{eff} = 8.73\ \mu_B$/Mn, which is slightly higher than the theoretical value of 5.92 for high-spin Mn^{2+} (d^5, $t_{2g}^3e_g^2$, S = 5/2). This kind of higher μ_{eff} values are widely noticed in many cathode materials.[24] Overall, the magnetic susceptibility study reveals long-range antiferromagnetic (AFM) ordering in $Na_{2.44}Mn_{1.79}(SO_4)_3$ with $T_N = 3.4$ K having no evidence for any ferromagnetic (FM) component or magnetic frustration.

3.3 Electronic structure calculations:

The lattice parameters predicted by the DFT based electronic structure calculations reveal the values of *a*=12.80 Å, *b*=12.73 Å, *c*=6.62 Å and β=114.19°. These are in good agreement with the experimental values, ensuring that the chosen model is nicely describing the relative compound that has been experimentally synthesized. The average value of Mn-O bond for the full and half sodiated cases are 2.16 Å and 2.11 Å respectively, while the average value of S-O bond in both sodiated and half sodiated systems are 1.46 (+0.2) Å. The average distortion parameter is 0.027 and 0.039 for full and half sodiated compounds. The formulation to compute the Open Circuit Voltage (OCV) is as follows:

$$V = -|E(Na_2Mn_2(SO_4)_3) - E(Na) - E(NaMn_2(SO_4)_3)|$$

Figure 9 show the projected density of state (pDOS) in each atom for $Na_2Mn_2(SO_4)_3$ and $NaMn_2(SO_4)_3$ systems respectively. The results follow the general trend of currently used cathode materials.[25-27] Sulfur contributions are observed in

more deep energies of the pDOS (between -9 eV to -7 eV). It reflects the fact that the hybridization between oxygen and sulfur atoms is forming strong covalent bonds. Most part of the pDOS in the energy range from -6 eV to -1 eV, the contribution comes from oxygen *p* states and Mn *d* states. In the close vicinity of the Fermi level and in the conduction band bottom, the contributions from *d* states of Mn centers are dominating with the band gap value 6.1 eV. The desodiation reaction is accompanied with a band gap reduction of 0.27 eV. Moreover, the magnetization per Mn center undergoes a change from 4.6 μ_B to 4.28 μ_B with high spin solution in the sodiated and desodiated cases. It indicates that the oxidation reaction is effectively occurring in the Mn transition metals where each Mn ion is contributing with half electron for the battery reaction. The redox potential energy (vs. Na/Na^+) is also evaluated for the half-desodiation reaction reaching a value of 4.4 V, which is 0.6 V higher than isostructural Fe-based (3.8 V) *alluaudite* cathode. It is a reasonable increment value observed in other polyanionic systems (e.g. $Na_2MnP_2O_7$ at 3.6 V vis-à-vis $Na_2FeP_2O_7$ at 3 V).[28] Owing to the lack of safe (organic) electrolytes, we were unable to experimentally observed the high Mn^{3+}/Mn^{2+} redox activity in the target compound. With the advent of new electrolytes with large potential window, $Na_{2+2x}Mn_{2-x}(SO_4)_3$ has potential to be exploited as a promising high-voltage cathode for sodium batteries.

Conclusion:

To summarise, we have discovered and solved the crystal structure of a novel *alluaudite* structured $Na_{2+2x}Mn_{2-x}(SO_4)_3$ (x = 0.22) compound, which marks the first ever Mn-containing SO_4-based *alluaudite* material. Adopting a monoclinic (*C*2/*c*) framework isotypical to the Fe-homologue, it is built from distorted MnO_6 octahedral blocks showing long range antiferromagnetic ordering at very low temperature of 3.4 K. This off-stoichiometric compound offers large tunnels for possible Na^+-migration. As per DFT study, it can facilitate efficient Na^+ (de)insertion involving Mn^{3+}/Mn^{2+} redox activity centered at 4.4 V (vs. Na/Na^+). Owing to lack to electrolytes stable upto high-voltage (ca. 5 V), it is difficult to currently implement $Na_{2+2x}Mn_{2-x}(SO_4)_3$ in practice, but it attests the richness of sulphate chemistry in designing novel insertion materials for rechargeable batteries.

Acknowledgements:

The authors are grateful to S. Ghara and Prof. A. Sundaresan (JNCASR, Bangalore) for carrying out magnetic characterization. The authors thank Department of Science and Technology (DST), Govt. of India for financial support under the aegis of Solar Energy Research Initiative (SERI) programme (DST/TMC/SERI/FR/169). DD thanks Ministry of Human Resource Development (MHRD) for financial support. RBA, SC and RA would like to acknowledge the Erasmus Mundus for a doctoral fellowship, Carl Tryggers Stiftelse for Vetenskaplig Forskning (CTS), Swedish Research Council (VR), Swedish Energy Agency & STandUP for financial support. SNIC, HPC2N and UPPMAX are acknowledged for providing computing time. The crystal structure was illustrated with the VESTA program.[29]

Reference:

1 N. Yabuuchi, K. Kubota, M. Dahbi and S. Komaba, *Chem. Rev.*, 2014, **114**, 11636.

2 C. Delmas, J. J. Braconnier, C. Fouassier and P. Hagenmuller, *Solid State Ionics*, 1981, **4**, 165.

3 A. K. Padhi, V. Manivannan and J. B. Goodenough, *J. Electrochem. Soc.*, 1998, **45**, 1518.

4 P. Barpanda, M. Ati, B. C. Melot, G. Rousse, J. N. Chotard, M. L. Doublet, M. T. Sougrati, S. A. Corr, J. C. Jumas and J. M. Tarascon, *Nat. Mater.*, 2011, **10**, 772.

5 M. Ati, B. C. Melot, G. Rousse, J. N. Chotard, P. Barpanda and J. M. Tarascon, *Angew. Chem. Int. Ed.*, 2011, **50**, 10574.

6 P. Barpanda, *Isr. J. Chem.*, 2015, **55**, 537.

7 P. Barpanda, G. Oyama, S. Nishimura, S. C. Chung and A. Yamada, *Nat. Commun.*, 2014, **5**, 4358.

8 J. Ming, P. Barpanda, S. Nishimura, M. Okubo and A. Yamada, *Electrochem. Commun.*, 2015, **51**, 19.

9 H. M. Rietveld, *J. Appl. Crystallogr.*, 1969, **2**, 65.

10 A. C. Larson and R. B. Von Dreele, General structure analysis system (GSAS); Los Alamos National Laboratory Report, LAUR 86-748; Los Alamos National Laboratory, NM, 1994.

11 B. H. Toby, *J. Appl. Crystallogr.*, 2001, **34**, 210.

12 G. Kresse and J. Hafner, *Phys. Rev. B*., 1993, **47**, 558.

13 G. Kresse and J. Hafner, *Phys. Rev. B.*, 1996, **54**, 11169.

14 J. P. Perdew, K. Burke and M. Ernzerhof, *Phys. Rev. Lett.*,1996, **77**, 3865.

15 S. L. Dudarev, G. A. Botton, S. Y. Savrasov, C. J. Humphreys and A. P. Sutton, *Phys. Rev. B*., 1998, **57**, 1505.

16 T. Mueller, G. Hautier, A. Jain and G. Ceder, *Chem. Mater.*, 2011, **23**, 3854.

17 J. Heyd, G. E. Scuseria and M. Ernzerhof, *J. Chem. Phys.*, 2003, **118**, 8207.

18 J. Heyd, G. E. Scuseria and M. Ernzerhof, *J. Chem. Phys.*, 2006, **124**, 219906.

19 K. Trad, D. Carlier, L. Croguennec, A. Wattiaux, M. B. Amara and C. Delmas, *Chem. Mater.*, 2010, **22**, 5554.

20 R. D. Shannon, *Acta Cryst. A*, 1976, **32**, 751.

21 I. D. Brown and D. Altermatt, *Acta Cryst. B*, 1985, **41**, 244.

22 P. Barpanda, N. Recham, J. N. Chotard, K. Djellab, W. Walker, M. Armand and J. M. Tarascon, *J. Mater. Chem.*, 2010, **20**, 1659.

23 P. Barpanda, J. N. Chotard, N. Recham, C. Delacourt, M. Ati, L. Dupont, M. Armand and J. M. Tarascon, *Inorg. Chem.*, 2010, **49**, 7401.

24 C. M. Julien, A. Ait-Salah, A. Mauger and F. Gendron, *Ionics*, 2006, **12**, 21.

25 C. Frayret, A. Villesuzanne, N. Spaldin, E. Bousquet, J. Chotard, N. Recham and J. M. Tarascon, *Phys. Chem. Chem. Phys.*, 2010, **12**, 15512.

26 S. C. Chung, P. Barpanda, S. Nishimura, Y. Yamada and A. Yamada, *Phys. Chem. Chem. Phys.*, 2012, **14**, 8678.

27 F. Zhou, M. Cococcioni, C. A. Marianetti, D. Morgan, and G. Ceder, *Phys. Rev. B*, 2004, **70**, 235121.

28 P. Barpanda, T. Ye, M. Avdeev, S. C. Chung and A. Yamada, *J. Mater. Chem. A*, 2013, **1**, 4194.

29 K. Momma and F. Izumi, *J. Appl. Crystallogr.*, 2011, **44**, 1272.

Table 1: Crystallographic data and atomic positions of $Na_{2+2x}Mn_{2-x}(SO_4)_3$ obtained from Rietveld refinement of high-resolution XRD data (λ = 1.5418 Å) at 298 K. Bond valence sum (BVS) values are also indicated.

Formula [molecular weight]	$Na_{2.44}Mn_{1.79}(SO_4)_3$ [437.657 g/mol]
Crystal system	Monoclinic
Space group	*C*2/*c* (#15)
Unit cell parameters (Å)	a = 12.809(1), b = 12.956(1), c = 6.579(0) β = 115.765(2)°, Z = 4
Unit cell volume ($Å^3$)	983.32(8)
Theoretical density (g/cm^3)	1.786
R values	R_p = 21.9%, R_{wp} = 31.3%, *R* (I, hkl) = 8.95%

Atom	Site	*x*	*y*	*z*	Occupancy	U_{iso} ($A^{0\,2}$)	BVS
Na1	4	0.0000	0.7677 (1)	0.2500	1.00	0.0170(1)	1.2190
Na2	4	0.0000	0.0000	0.0000	0.64(1)	0.0241(1)	0.9880
Na3	4	0.0000	0.4803(1)	0.2500	0.80(1)	0.0253(1)	0.5832
Mn1	8	0.7295(1)	0.1520(1)	0.1495(1)	0.89(1)	0.0065(1)	1.7236
S1	4	0.0000	0.2146(1)	0.2500	1.00	0.0214(1)	5.9153
O11	8	0.0748(1)	0.8572(1)	0.7059(1)	1.00	0.0218(1)	2.3012
O12	8	0.4485(1)	0.2131(1)	0.5412(1)	1.00	0.0300(1)	1.8687
S2	8	0.7621(1)	0.5994(1)	0.8690(1)	1.00	0.0171(1)	5.3453
O21	8	0.7768(1)	0.6703(1)	0.6962(1)	1.00	0.0419(1)	1.8375
O22	8	0.3388(1)	0.9927(1)	0.3752(1)	1.00	0.0214(1)	1.9632
O23	8	0.3675(1)	0.5838(1)	0.6771(1)	1.00	0.0711(1)	1.7359
O24	8	0.3315(1)	0.1588(1)	0.0839(1)	1.00	0.0131(1)	1.9419

List of Figures:

Figure 1: Rietveld fit of powder X-ray diffraction pattern (λ_{Cu} = 1.5418 Å) of $Na_{2+2x}Mn_{2-x}(SO_4)_3$ showing the experimental profile (red dots), calculated pattern (black line), their difference (blue line) and the Bragg diffraction positions (blue ticks).

Figure 2: Structural illustration of $Na_{2+2x}Mn_{2-x}(SO_4)_3$ alluaudite. (a) Projection along c axis showing MnO_6 octahedral (pink) and SO_4 tetrahedral (yellow) building blocks accommodating Na ions into three distinct sites (marked as Na1, Na2, Na3) inside large tunnels. (b) Local surrounding of Mn atoms, and (c) local environment of the three distinct Na sites (Na1, Na2, Na3) in the alluaudite framework.

Figure 3: Morphology of as-synthesized alluaudite $Na_{2+2x}Mn_{2-x}(SO_4)_3$. (a-d) SEM images showing micrometric particles consisting of nanometric spherical particles. (d-f) TEM micrographs of spherical nanoparticles and (inset of f) representative SAED pattern.

Figure 4: Elemental analysis of *alluaudite* $Na_{2+2x}Mn_{2-x}(SO_4)_3$. (a) representative micrometric agglomerate of particles, (b) EDX spectrum capturing signals of constituent elements, and elemental mapping showing the uniform distribution of (c) Na, (d) Mn, (e) S and (f) O atoms.

Figure 5: FT-infrared spectrum of alluaudite $Na_{2+2x}Mn_{2-x}(SO_4)_3$ depicting distinct vibration bands resulting from constituent SO_4 building blocks. The peak ~2300 cm^{-1} is a system peak arising from background/ sample holder.

Figure 6: TGA graph showing the thermal stability of $Na_{2+2x}Mn_{2-x}(SO_4)_3$ and isostructural $Na_{2+2x}Fe_{2-x}(SO_4)_3$ until 900 °C.

Figure 7: Magnetization (M-H) curves acquired (a) at 300 K and (b) at 2 K.

Figure 8: Temperature dependence of the magnetization (M) of $Na_{2+2x}Mn_{2-x}(SO_4)_3$ measured in field cooled (FC) mode. Inset image shows the antiferromagnetic ordering around 3.4 K.

Figure 9: Projected and total density of states of (top) $Na_2Mn_2(SO_4)_3$ and (bottom) $NaMn_2(SO_4)_3$. Red is representing the summed contribution of the Mn atoms. Blue is representing the sulfur atoms contribution and green the oxygen atoms contribution. Gray is the total DOS.

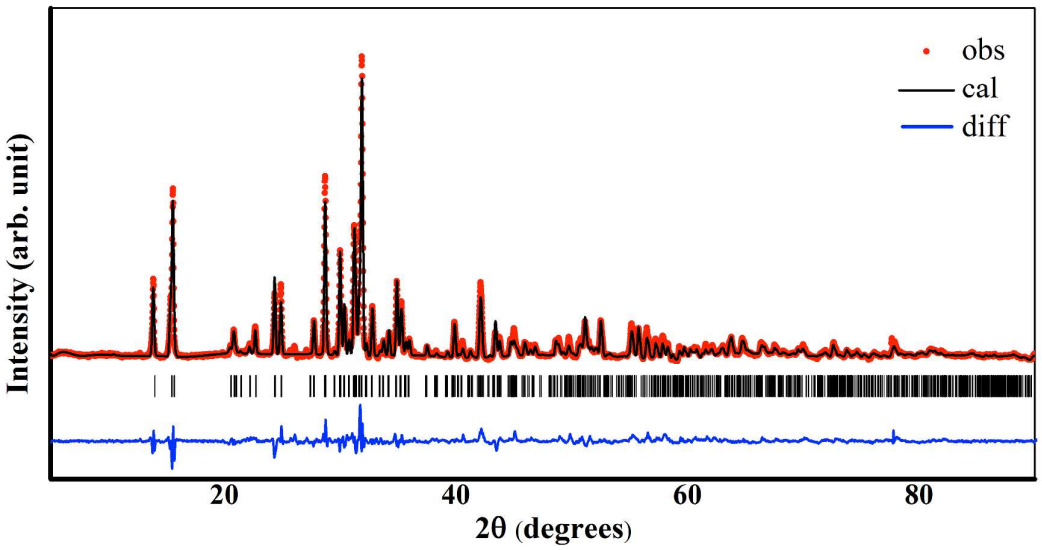

Figure 1

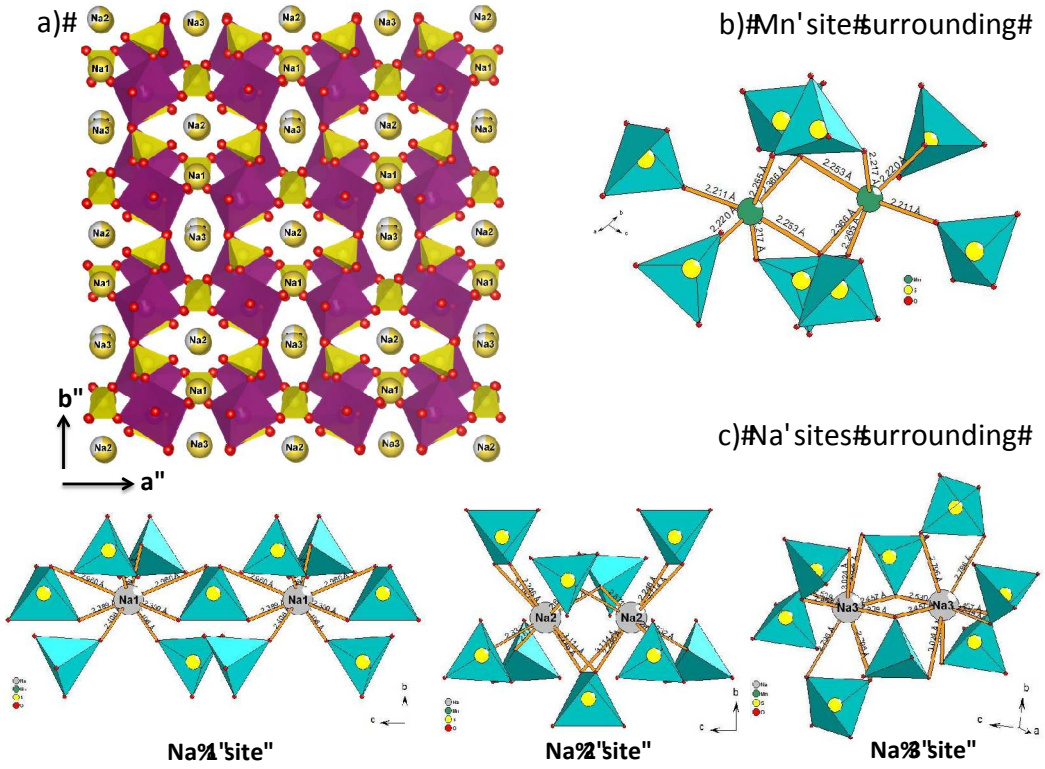

Figure 2

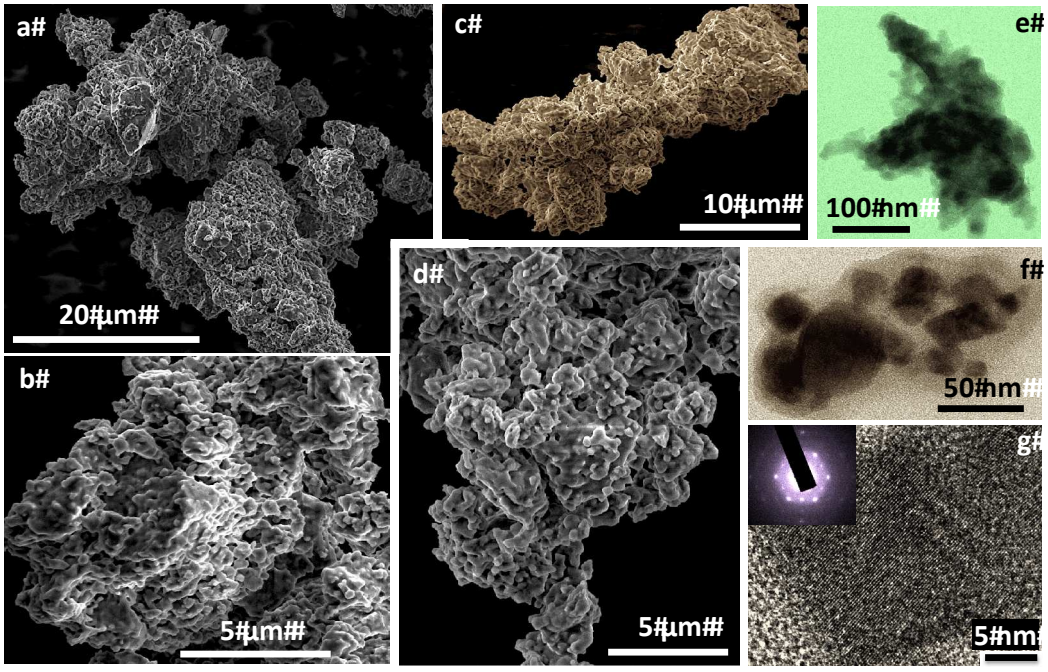

Figure 3:

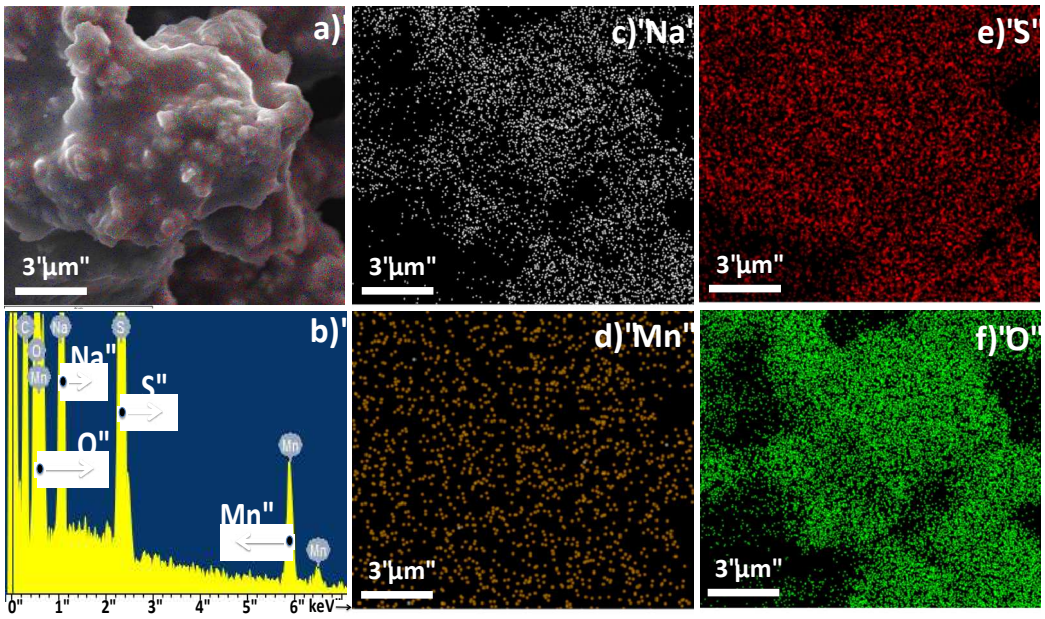

Figure 4:

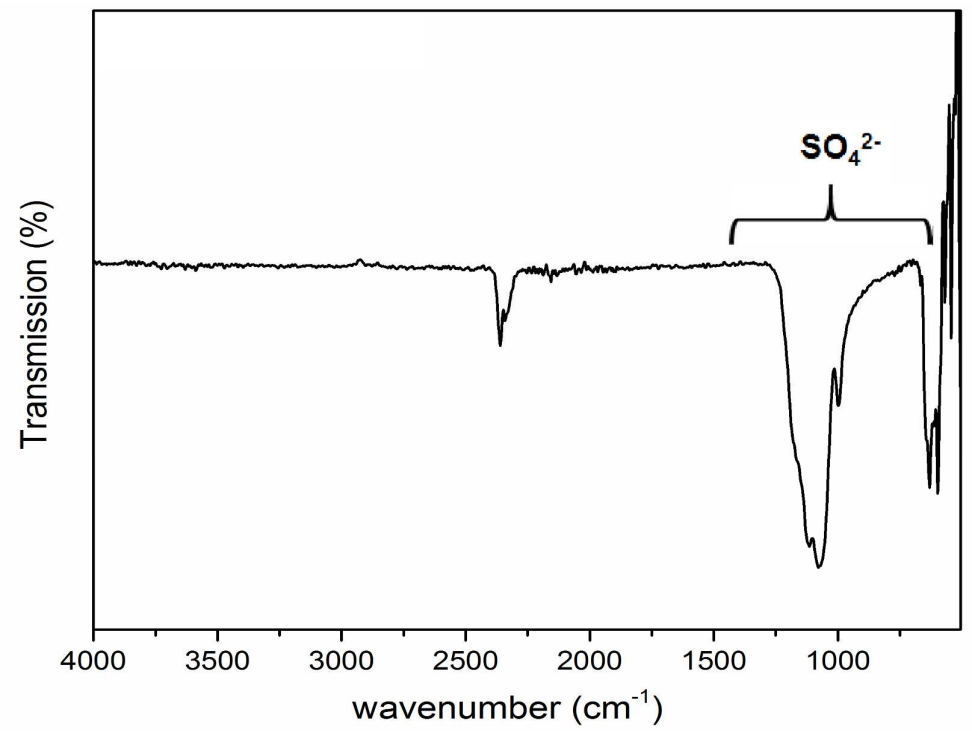

Figure 5:

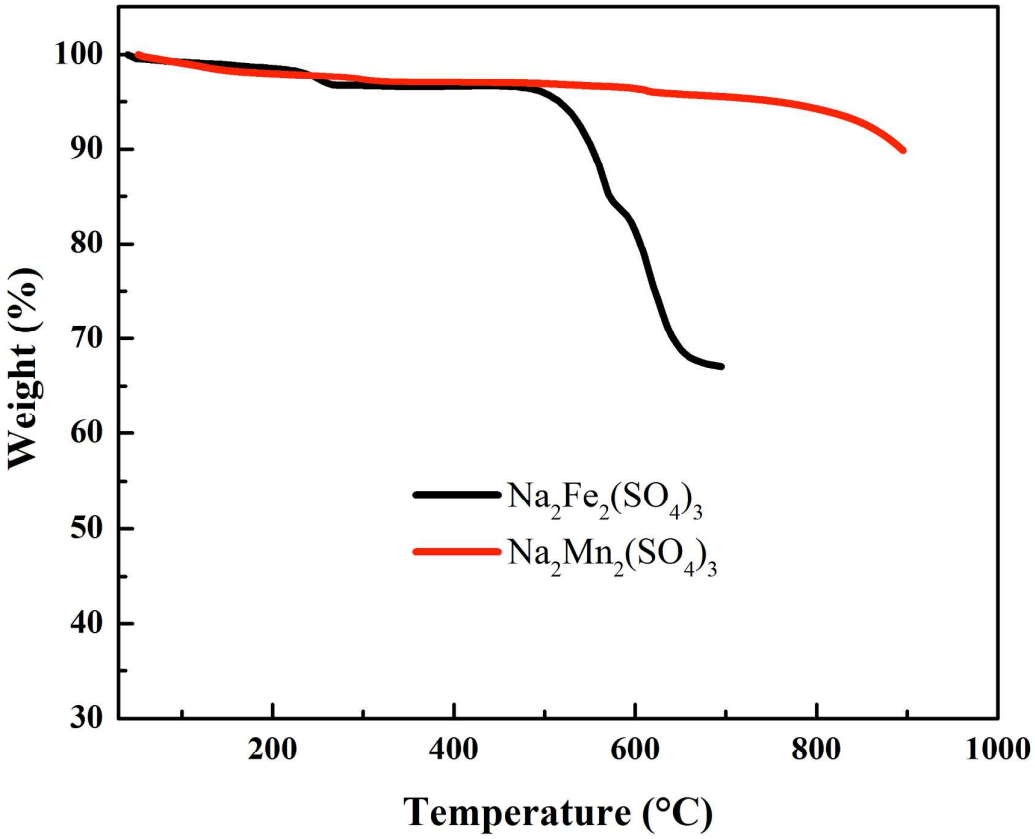

Figure 6:

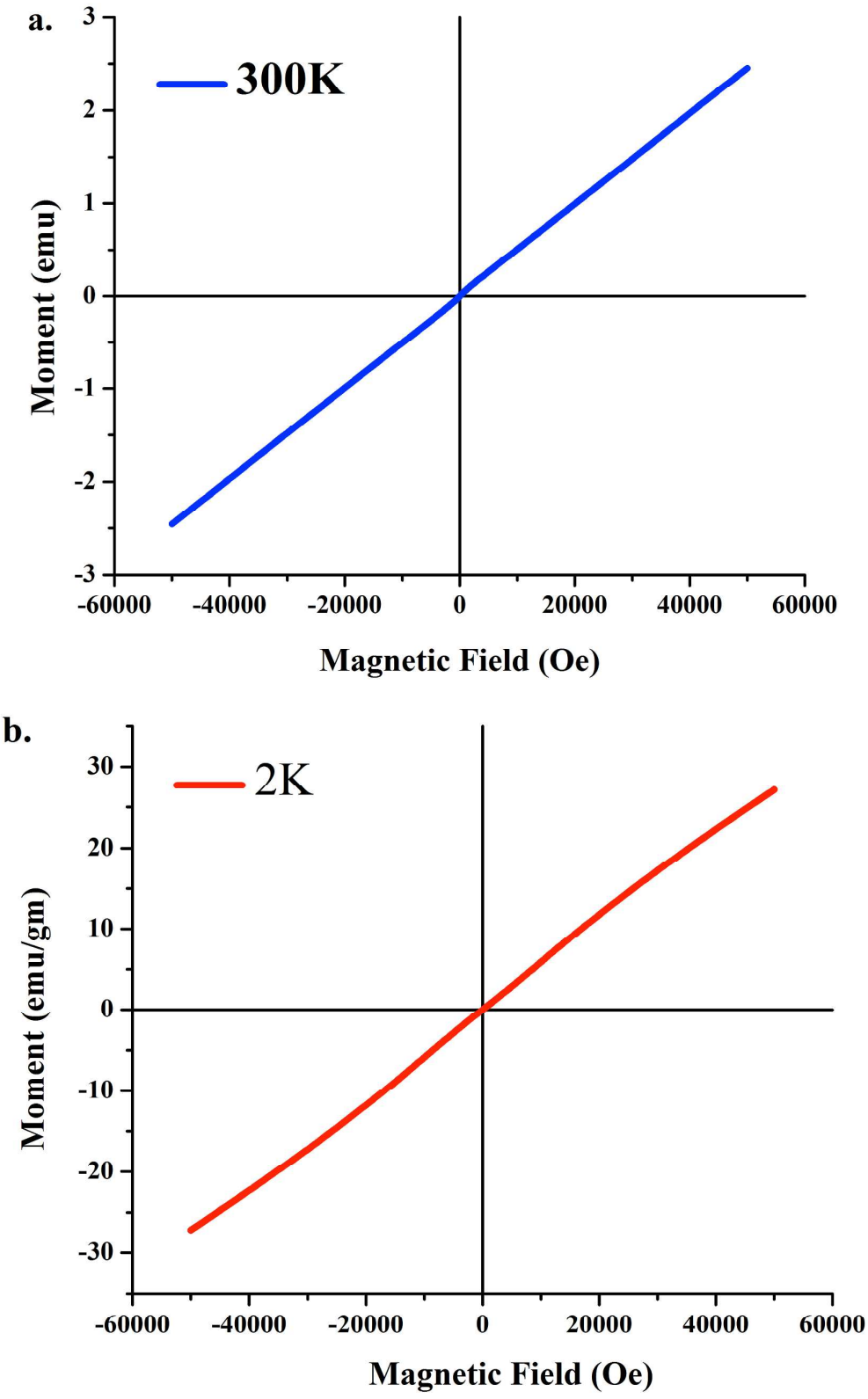

Figure 7:

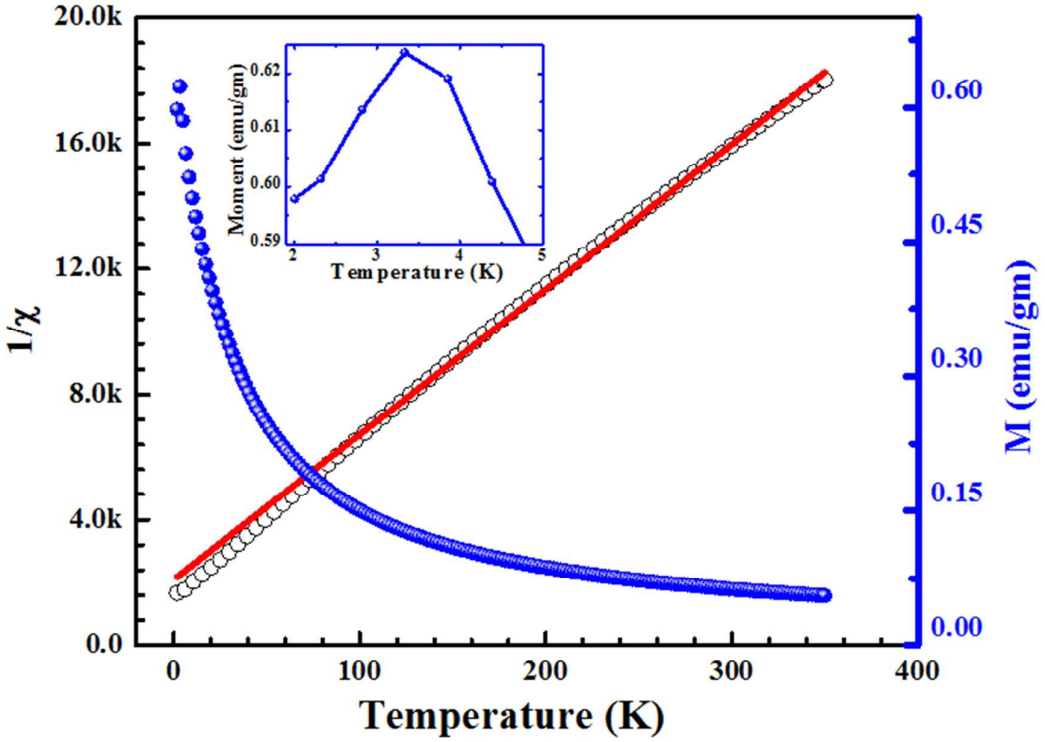

Figure 8:

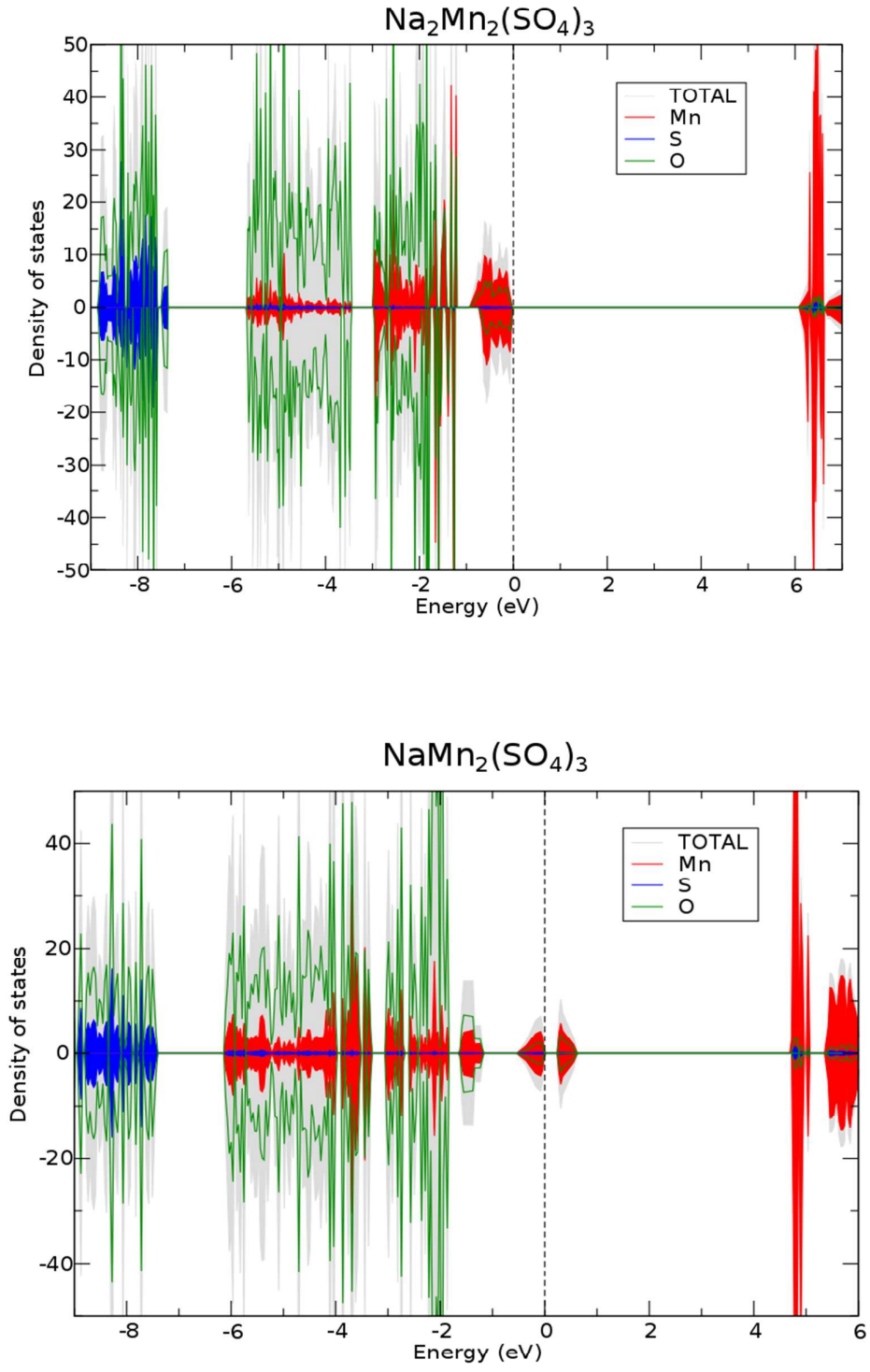

Figure 9: